Magnetically "tagged" nuclear relaxation in superionic conductors

S. P. Vernon,* P. Thayamballi,† R. D. Hogg,‡ D. Hone, and V. Jaccarino
Department of Physics, University of California, Santa Barbara, California 93106
(Received 24 March 1981; revised manuscript received 26 May 1981)

Introducing paramagnetic atoms into a superionic conductor may produce large, temperature-dependent effects on the transverse T_2^{-1} and longitudinal T_1^{-1} relaxation rates of the NMR of the nuclei of the diffusing ions. Such effects have been observed for the first time in a study of the ^{19}F NMR in PbF_2, substitutionally doped with Mn^{2+} ions at concentrations c ranging from 0.01 to 1 mole%. The relaxation induced by the ^{19}F-Mn^{2+} near-neighbor-transferred hyperfine interaction, $\vec{I}\cdot\vec{A}\cdot\vec{S}$, results in a single peak in T_2^{-1} vs T and two peaks in T_1^{-1} vs T, with the rates proportional to c. A unified treatment of both the statistical aspects of the F^- ion motion and the dynamical evolution of the ^{19}F magnetization during the encounters with the Mn^{2+} spins is given within the framework of an "impact" model theory. This approach is contrasted with an earlier perturbative treatment by Richards and is shown to differ from it in several important respects. With the help of recently measured values of $\tilde{A}$ for Mn^{2+} in PbF_2 and estimates of the Mn^{2+} electronic spin-lattice relaxation obtained from EPR studies, a comparison between theory and experiment is made. Agreement is found at all but the highest temperatures for T_2^{-1}, indicating a larger spectral density of low-frequency fluctuations than is expected.

I. INTRODUCTION

Superionic conductors (or solid electrolytes) are a class of solids that exhibit large ionic conductivities, $\sigma \simeq 1\ (\Omega\,\mathrm{cm})^{-1}$ well below the melting point, typical of the values found in molten salts. NMR has proven to be a powerful tool in extracting the microscopic character of the ion motion in these materials.[1,2] In the present work we introduce[3–5] a new magnetic "tagging" technique and apply it to an NMR study of the fundamental superionic conductor PbF_2. A theory is developed to interpret the variety of experimental results that have been obtained.

PbF_2 was chosen for several reasons: It is among the best of the *anion* conductors, achieving a conductivity of $1\ (\Omega\,\mathrm{cm})^{-1}$ at $T = 500\,^\circ\mathrm{C}$, well below its melting point ($T_m = 823\,^\circ\mathrm{C}$), and has been studied extensively using a variety of experimental techniques.[6–9] It crystallizes in the fluorite structure (space group $Fm3m$) with the Pb^{2+} cations arranged on a fcc lattice ($a_0 = 5.96$ Å) and the F^- anions at the eight equivalent $\frac{1}{4}\frac{1}{4}\frac{1}{4}$ positions forming a simple cubic (sc) sublattice of side $a_0/2$. Alternately, one may consider the cations as occupying the body centered positions in *alternate* cubes in the sc lattice formed by the anions (see Fig. 1). From the viewpoint of NMR, PbF_2 is an excellent candidate. The mobile ion nucleus, ^{19}F, with $I = \frac{1}{2}$, has a large gyromagnetic ratio g_I and is 100% abundant. ^{207}Pb, the only stable $I \neq 0$ lead isotope also has $I = \frac{1}{2}$, but a much smaller g_I and a natural abundance of 23%. Importantly no quadrupolar effects complicate the nuclear relaxation phenomena in either case. Lastly, PbF_2 provides an excellent host for magnetic "tagging," allowing the introduction of Mn^{2+} for Pb^{2+}, substitutionally, in amounts exceeding 1% while preserving the fluorite structure. This has made possible both ^{19}F NMR and Mn^{2+} EPR complementary studies of the ion motion as a function of temperature.[3–5,10]

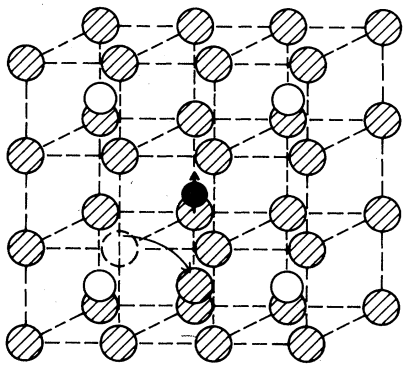

FIG. 1. β-PbF_2 structure. The F^- ions (shaded circles) reside on a simple cubic sublattice and the Pb^{2+} ions (open circles) occupy the body centered positions in alternate cubes. A paramagnetic Mn^{2+} impurity (solid circle), introduced substitutionally for the Pb^{2+}, is shown in the center of the figure. Thermally activated Frenkel disorder of the anion sublattice transports the F^- to the Mn^{2+} NN positions. ^{19}F NMR relaxation occurs through the transferred hfs interaction $\vec{I}\cdot\vec{A}\cdot\vec{S}$ between a Mn^{2+} spin $\vec{S}$ and its NN F^- nuclei. This is the dominant relaxation process above 400 K in the Mn^{2+}-doped PbF_2.

An extensive investigation of the ^{19}F NMR in nominally pure PbF_2 already exists,[8] but we will see that the nuclear relaxation is highly sensitive to magnetic contamination. Inadvertent magnetic "tagging" at a level as small as 1 ppm is a likely source of some features of the observations of Ref. 8. Indeed, all of the relaxation phenomena to be considered in the following sections are dominated by the presence of the Mn^{2+} ions (above 400 K) when their concentration exceeds a few ppm.

In Sec. II we briefly describe the magnetic "tagging" technique. Section III deals with the experimental procedures and apparatus. Section IV gives the experimental results on the measurements of the transverse T_2^{-1} and longitudinal T_1^{-1} relaxation rates of the ^{19}F NMR from 300 to 1050 K, at frequencies from 8 to 90 MHz and Mn^{2+} concentrations ranging from 0.01 to slightly less than 1 mole%.

In Sec. V a theoretical interpretation of the observed relaxation phenomena is given. Richards[11] has developed an elegant theory of nuclear relaxation by paramagnetic impurities in the superionic conductors. It utilizes the Kubo-Tomita[12] perturbation method to construct the time evolution of the nuclear magnetization relaxation function to obtain both T_1 and T_2. Richards's model suffers in two respects, first with regard to the use of a perturbation approach, which we shall show is not valid for Mn:PbF_2 at the lower end of the temperature region at which it has been used, and second, because of the inadequate statistical treatment of the F^- diffusion processes. Consequently, we have developed an alternative approach to the ^{19}F NMR relaxation in Mn:PbF_2, the "impact model," which incorporates a detailed and nonperturbative treatment of the nearest-neighbor Mn-F transferred hyperfine interaction and an improved statistical treatment of the F^- diffusion. The authors were led to this approach because of the similarities of the ^{19}F NMR relaxation in Mn:PbF_2 to the lifetime-limited linewidths observed in the optical spectra in dilute gases, where the atomic relaxation results from "hard" collisions between particles. Kubo has successfully modeled relaxation in these systems using an impact theory appropriate to the strong collision[13] regime.

In Sec. VI the impact model predictions for T_1^{-1} vs T and T_2^{-1} vs T, obtained using "best" values of the parameters that enter into the theory, are presented. These results are compared with the experimental observations and are contrasted with those obtained from a perturbative treatment.

II. MAGNETIC "TAGGING" AS APPLIED TO NMR IN SUPERIONIC CONDUCTORS

Consider an ionic conductor in which only the anions readily diffuse at temperatures well below the melting point while the cations remain essentially fixed (as in the example to be discussed, PbF_2). Suppose a small fraction of the cations are substitutionally replaced with paramagnetic atoms (e.g., Mn^{2+} substituted for Pb^{2+} in PbF_2) and that a strong transferred hfs interaction exists between the paramagnetic atom and the anions *only when they are nearest neighbors.* Then the anion nuclear moment is subjected to a time-varying, random magnetic field as it diffuses through the crystal, which results in the dynamic relaxation of the nuclear magnetization. We refer to this as the magnetic "tagging" technique. It clearly will be a sensitive, microscopic probe of the detailed paths by which anion diffusion takes place and will depend upon, in addition to the lattice topology, the F^- hopping rate W, the hfs interaction $\vec{I}\cdot\vec{A}\cdot\vec{S}$, the nuclear ($\omega_n$) and electronic ($\omega_e$) Larmor frequencies and the electronic spin relaxation rate ($1/\tau_{sl}$) and on the concentration (c) of paramagnetic spins.

The effects produced by magnetic "tagging" are most dramatically seen in the superionic conductor, because the anion hopping rate W changes by many orders of magnitude as the temperature is varied and can even be made to exceed the Larmor frequency of the paramagnetic spin. But magnetic "tagging" should be apparent even in ordinary ionic conductors, provided only that the ionic self-diffusion rate exceeds the nuclear spin diffusion[14–16] rate.

Perhaps the simplest effect associated with magnetic "tagging" is that which is seen on the linewidth or T_2 of the ^{19}F NMR in Mn:PbF_2 at moderately low temperatures. If the spin memory of a given ^{19}F suffers total dephasing when it "encounters" just one paramagnetic spin, which requires that the change in the local field δH satisfies $\delta H \gg \pi/\gamma\tau$, with τ being the encounter time, then $T_2 = K\tau/c$, with K a constant of the order of unity that depends on the lattice topology and c the paramagnetic ion concentration.[3] This remarkable fact that T_2 (and T_1) are independent of the coupling constants of the problem (in the temperature region where the above inequality holds) is an intriguing result of this study.

The initial choice of $Mn^{2+}3d^5$ for the paramagnetic ion was dictated by the need for a "slow" relaxer. If the paramagnetic ion spin-lattice relaxation rate $(\tau_{sl})^{-1}$ exceeded the hopping rate, then the spectral density of the local field fluctuations would be determined by it and not by the ion diffusion. Indeed, just this situation is seen in our study of the ^{19}F NMR in $KCoF_3$ where $(\tau_{sl})^{-1}$ even exceeds the exchange frequency.[17] The effects of introducing fast relaxing ions in a superionic conductor will be given in a later paper.[18]

III. EXPERIMENTAL PROCEDURES

Very-high-purity PbF_2 powder[19] was placed in open graphite crucibles and baked at 300 °C in vacuum for

2–3 days to remove absorbed contaminants (primarily H_2O). The powder was heated above the melting point ($T_m = 823\,^{\circ}C$) for 15 min in an argon atmosphere, then rapidly cooled. The resultant polycrystalline material was mixed with crystalline MnF_2, ground to powder, placed in a newly pyrolized[20] open graphite a crucible and maintained at 250 °C in a flow of HF gas for 2 h. The crucible was capped and raised above T_m for 15–30 min in HF, then rapidly cooled. No discernible weight loss occurred if this procedure was followed.

The site symmetry of the Mn^{2+}, the randomicity of its distribution and the absolute impurity concentration are essential to the interpretation of the ^{19}F NMR experimental results. A series of NMR, EPR, and magnetic susceptibility measurements[5,10,23] indicate that the Mn^{2+} reside in eightfold anion coordinated lattice sites and probably enter the PbF_2 structure substitutionally for Pb^{2+}. As much as 2 mole% Mn^{2+} is soluble in PbF_2 and polycrystalline material displays negligible variation in the Mn^{2+} distribution. However, single crystals of Mn:PbF_2 exhibit gradients in c as large as 50% per cm. Because of this limitation no systematic NMR study of single-crystal Mn:PbF_2 was made. Finally, these measurements show no evidence of clustering of the impurities.

During the high-temperature runs the samples were contained in pyrolitic boron crucibles, fitted with graphite caps, in an atmosphere of dry nitrogen. These precautions were necessary because of the extreme reactivity of PbF_2 with oxygen bearing compounds and permitted reproducible ^{19}F NMR relaxation rate measurements after repeated temperature cycling. However, sample deterioration occurred if the samples were maintained near T_m for prolonged periods. To minimize this effect, the final measurements were made in a single temperature cycle, with the frequency-dependent measurements carried out at a fixed T.

The ^{19}F NMR relaxation rate measurements were made using standard pulse sequences, with the computer controlled spectrometer schematically illustrated in Fig. 2. The importance of minimizing the duration of the high-T experiments necessitated the construction of a special high-Q, variable-temperature resonator, tunable over more than a decade in ω_0. The broad tuning capability necessarily compromises the performance at a given frequency. Consequently, over the frequency region between 8 and 90 MHz the ambient temperature signal-to-noise ratio varies from 5 to 100 for ^{19}F in PbF_2, the Q varies from 10 to 90, and the receiver recovery time ranges from 7 to 3 μsec. Temperature measurements were made with a Cr-Al thermocouple in good thermal contact with the crucible. The temperature was uniform over the sample volume and stable to within ±1 K. A detailed discussion of the spectrometer and resonator is given elsewhere.[5]

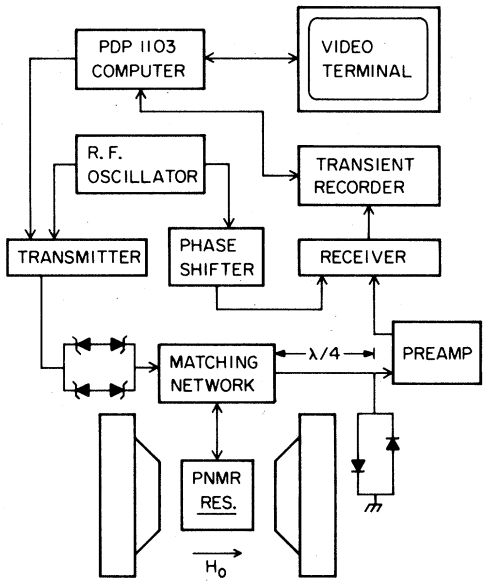

FIG. 2. Schematic diagram of the computer-controlled, transient NMR spectrometer. In addition to providing gating waveforms for both the transmitter and transient recorder, the computer signal averages the accumulated data and fits them to an exponential. The λ/4 coaxial cable and crossed diodes are a resonant transmission line which protect the preamplifier from overload during the high power pulse.

IV. EXPERIMENTAL RESULTS

In the initial paper[3] on magnetic "tagging" we reported measurements of the *linewidth* of the ^{19}F NMR in Mn:PbF_2, as a function of temperature and Mn concentration, using continuous wave techniques. Here we present measurements of T_1 and T_2 using transient techniques.

Three samples of Mn:PbF_2 were prepared and characterized following the procedures described in Sec. III. Samples "A" and "C" were polycrystalline line specimens with *nominal* concentrations of 1.0 and 0.01 mole% Mn^{2+}, respectively. Sample "B" was obtained from a large single crystal of Mn:PbF_2 (nominal $c = 0.1$ mole%). The measured concentrations for samples A, B, and C are 0.986 ± 0.005, 0.05 ± 0.015, 0.015 ± 0.005 mole%, respectively. The measured c for sample B has a larger uncertainty than that of the polycrystalline materials, for reasons discussed in Sec. III.

Figure 3 shows T_1^{-1} and T_2^{-1} vs T for sample C. T_2 was measured at $\omega_0 = (2\pi)87.17$ MHz and T_1 was measured at three frequencies, $\omega_0 = (2\pi)(8.8, 31.15,$ and 87.17 MHz). Below 300 K the rigid lattice nuclear dipole–dipole interaction is the source of line

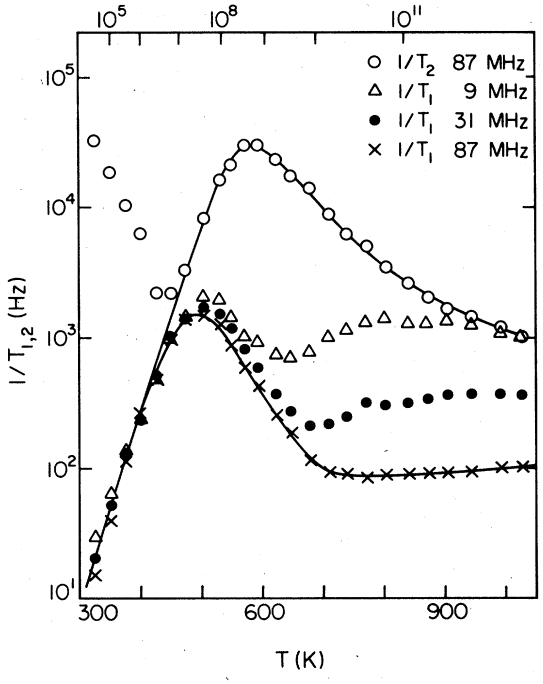

FIG. 3. Observed dependence of the ^{19}F NMR relaxation rates T_1^{-1} and T_2^{-1} in sample C (0.015 ± 0.005 mole%) on temperature. T_1 was measured at three frequencies, $\omega_0/2\pi = 8.88$, 31.15, and 87.17 MHz and T_2 at $\omega_0/2\pi = 87.17$ MHz. Note that there is a single peak in T_2^{-1} vs T whereas T_1^{-1} exhibits two peaks, with the broader, high temperature one being a strong function of field (or frequency). The solid lines are guides to the eye. The ion hopping rate W is indicated on the upper abscissa.

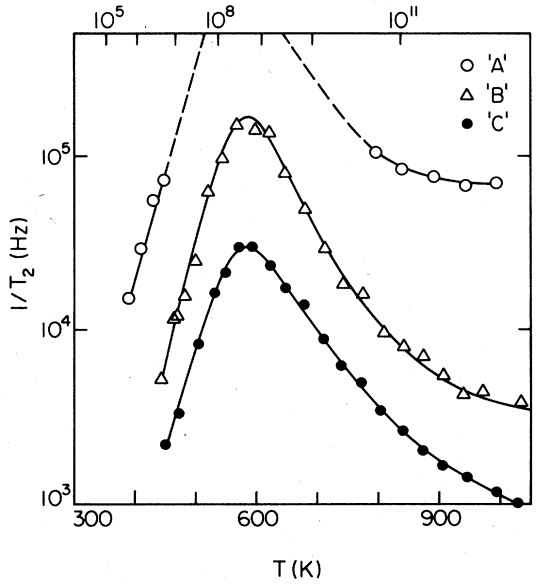

FIG. 4. Observed dependence of T_2^{-1} on temperature, at a fixed frequency ($\omega_0/2\pi \simeq 85$ MHz), for three different Mn^{2+} concentrations in PbF_2, with $c = 0.015 \pm 0.05$(C), 0.05 ± 0.015(B), and 0.984 ± 0.005(A) mole%. The effects of magnetic "tagging" are seen to be linear in c, within experimental error, for values of $c \ll 1$. Only partial data exist for the highest Mn^{2+} concentration because T_2 is less than the spectrometer dead time between 500 and 800 K. The solid lines are guides to the eye. The ion hopping rate W is indicated on the upper abscissa.

broadening and the decay of the transverse magnetization is Gaussian. Starting at 350 K, the F^- ion hopping causes the line to motionally narrow and the decay becomes increasingly exponential in character. At all temperatures above 380 K the decay is exponential, and since we are only interested here in the magnetic "tagging" effects, it is this region which will concern us. T_2^{-1} is observed to decrease with increasing T, until a minimum value is attained at approximately 420 K. Above this temperature T_2^{-1} increases with increasing T, reaching a maximum value at 600 K. Above 600 K T_2^{-1} decreases with increasing T up to the highest temperature investigated.

The measured T_1^{-1} increases with increasing T and rapidly passes from a low-T, frequency-dependent region to a frequency-independent one. This increase continues with increasing T, and reaches a maximum value at 500 K. At this point a slight frequency dependence is observed, with the peak rate largest for smallest ω_0. With further increase in temperature, T_1^{-1} exhibits a dramatic dependence on ω_0, with the rate largest for the smallest ω_0. The data are suggestive of an additional frequency-dependent T_1 process becoming important at elevated temperatures. In fact, the lowest frequency data actually pass through a second maximum at elevated temperatures, while the higher ω_0 data appear to be approaching a second maximum. At the highest T, with $\omega_0/2\pi = 8.88$ MHz, the longitudinal and transverse rates are equal, whereas at higher frequencies T_1^{-1} falls below T_2^{-1}. This indicates that the spectral density of the local field fluctuations is constant below 8 MHz, and decays to about 10% of its low-frequency value at 90 MHz. In the temperature region where T_2^{-1} increases, the data fall on the curve drawn through the frequency-independent T_1^{-1} points. This suggests that in this temperature region both relaxation rates result from a single mechanism.

We have measured these same quantities in samples A and B and find that the observed rates scale linearly (within experimental error) with c. This can be seen in Figs. 4 and 5. Only partial data exist for sample A as the NMR relaxation times for T between 450 and 800 K were shorter than the spectrometer recovery time.

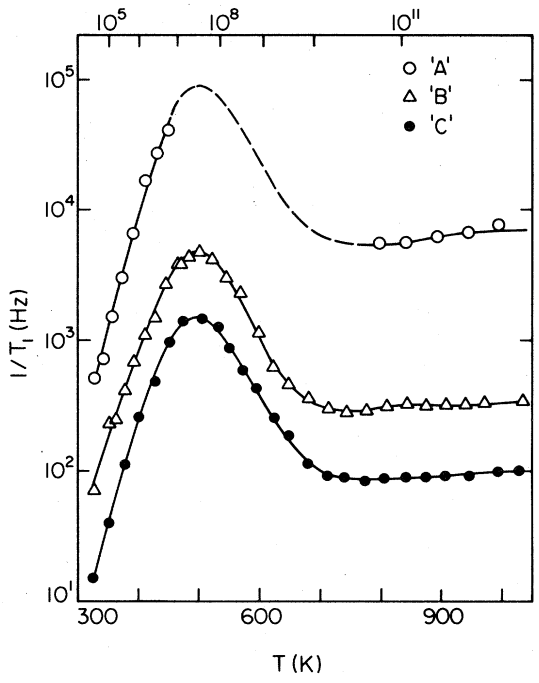

FIG. 5. Observed dependence of T_1^{-1} on temperature, at a fixed frequency ($\omega_0/2\pi \simeq 85$ MHz), for the same three Mn^{2+} concentrations given in Fig. 4. Again the effects of magnetic "tagging" are seen to be linear in c, within experimental error. Spectrometer dead time precludes measurements of T_1 in the 500 to 800 K region for the highest Mn concentration sample. The solid lines are guides to the eye. The ion hopping rate W is indicated on the upper abscissa.

V. THEORETICAL MODELS OF THE ^{19}F RELAXATION

At temperatures $T > 350$ K and Mn^{2+} concentrations $c > 10^{-5}$, the relaxation of the ^{19}F nuclear spins occurs primarily through the transferred hyperfine interaction $\vec{I} \cdot \tilde{A} \cdot \vec{S}$ that exists between a paramagnetic Mn^{2+} spin $\vec{S}$ and nearest-neighbor (NN) ^{19}F nuclei. Diffusion provides the mechanism by which the F^- ions are bodily transported to lattice positions NN to the Mn^{2+} and determines the residence time in these positions.

Richards[11] has developed a model of nuclear relaxation appropriate to this system, which we subsequently refer to as the average encounter model (AEM). Although the AEM exhibits features qualitatively similar to the observed ^{19}F nuclear relaxation in Mn:PbF_2, there are no self-consistently chosen values of the parameters influencing nuclear relaxation in Mn:PbF_2 for which quantitative agreement can be found for all of the observed relaxation rates. Moreover, there are fundamental shortcomings of the AEM which arise from two sources. The first is the use of Kubo-Tomita perturbation theory,[12] which is strictly valid only when the local field fluctuations producing the nuclear relaxation constitute a Gaussian random process, or when the fluctuations are small, so that the cumulant expansion may be terminated at the second order. In general, the dynamic interaction $\tilde{A}$ between the Mn^{2+} and ^{19}F does not satisfy either of these criteria. The second flaw in the AEM development is the statistical treatment of the F^- motion, which ignores the topological aspects of diffusion on the PbF_2 lattice.

We have developed an alternative approach to the nuclear relaxation which incorporates both a detailed, nonperturbative treatment of the NN interaction $\tilde{A}$ and a proper statistical approach to the F^- diffusion in PbF_2. The nonperturbative treatment is essential to the description of the low-temperature region ($T < 700$ K) where the magnitude of the interaction $|\tilde{A}|$, and the duration of the NN encounter τ_c, are such that $|\tilde{A}|\tau_c \gtrsim 1$, so that perturbation theory breaks down. This situation has similarities with the problem of the pressure broadening of optical lines in gases, where the collisions between the particles induce relaxation. In the latter case an "impact model" of the strong collisions[13] has been used to describe the observed linewidth dependence on pressure and collision cross section. A similar approach has been used in the theory applicable to the low- and zero-field relaxation behavior observed in muon spin rotation.[21] We have extended this model to the present problem. Before embarking on the impact model derivation, we briefly review the AEM with the dual purpose of quantifying the objections to the assumptions implicit in the AEM, and of facilitating a comparison between the two models.

A. Average encounter model

In the AEM, as in our model, the dominant interaction producing nuclear relaxation is the transferred hyperfine interaction between the Mn^{2+} spin and NN ^{19}F nuclei, and all others are neglected. While a ^{19}F is NN to a Mn^{2+} ion it experiences a time-dependent interaction

$$\mathcal{H}' = \sum_{\alpha,\beta} I_\alpha A_{\alpha\beta} S_\beta(t) \ , \tag{5.1}$$

with $\alpha, \beta = \pm, z$ denoting the transverse and longitudinal components, respectively. The time dependence of Eq. (5.1) arises both from F^- diffusion, which transports ^{19}F nuclei to lattice sites NN to the Mn^{2+}, and from the dynamical fluctuations of the electron spin. The Kubo-Tomita perturbation technique[12] is used to develop the equation of motion of $\tilde{I}_\alpha$ (I_α in the rotating frame) subject to the interaction $\mathcal{H}'$

$$\frac{d}{dt}\tilde{I}_\alpha(t) = i \sum_{\alpha',\beta'} A_{\alpha'\beta'} S_{\beta'}(t) [\tilde{I}_{\alpha'}(t), \tilde{I}_\alpha(t)] e^{-i\alpha'\omega_0 t} \ . \tag{5.2}$$

First integrating, then iterating this equation and averaging over both electronic spin and spatial coordinates, we obtain a relation, correct to second order in $A_{\alpha'\beta'}$ for $\tilde{I}_\alpha(t+\tau)$:

$$\tilde{I}_\alpha(t+\tau) \simeq \tilde{I}_\alpha(t)\exp\left[-\int_0^\tau dt'(\tau-t')G_\alpha(t')\right] . \quad (5.3)$$

The equations for the $G_\alpha(t)$ are given in the Appendix and differ slightly from those found in Ref. 11. They are functions of the $A_{\alpha\beta}$, the nuclear (ω_0) and electronic (ω_e) Larmor frequencies, and the electron-spin-relaxation rate $(\tau_{sl})^{-1}$. Thus, as a consequence of an encounter with a Mn^{2+} spin, of duration τ, $\tilde{I}(t)$ differs from its preencounter value $\tilde{I}(0)$ by the relation

$$\tilde{I}_\alpha(t) = f_\alpha(\tau)\tilde{I}_\alpha(0) \quad (5.4)$$

for $t > \tau$, where $f_\alpha(\tau)$ is defined by Eq. (5.3).

If n encounters with Mn^{2+} spins occur during a walk of length t, it follows that

$$\tilde{I}_\alpha(t) = \prod_{i=1}^{n} f_\alpha(\tau_i)\tilde{I}_\alpha(0) . \quad (5.5)$$

The normalized relaxation function $F_\alpha(t)$ of the macroscopic nuclear magnetization is given by

$$F_\alpha(t) = \left\langle\!\left\langle \prod_{i=1}^{n} f_\alpha(\tau_i) \right\rangle\!\right\rangle . \quad (5.6)$$

Two averages are involved in Eq. (5.6), one with respect to τ_i and another with respect to the number of encounters n. If the probability that a F^- encounters a Mn^{2+} more than once within an electron relaxation time is vanishingly small, then each encounter is a statistically independent event. The averaging simplifies:

$$F_\alpha(t) = \langle \langle f_\alpha(\tau_i)\rangle^n \rangle_n . \quad (5.7)$$

Since $We^{-W\tau}d\tau$ is the probability that an ion hopping at rate W will remain at a site for a time between τ and $\tau + d\tau$ before hopping away, one finds that

$$\langle f_\alpha(\tau_i)\rangle = W\int_0^\infty d\tau\, e^{-W\tau} f_\alpha(\tau) \equiv f_\alpha , \quad (5.8)$$

and

$$F_\alpha(t) = \sum_{n=0}^{\infty} P(n,t) f_\alpha^n . \quad (5.9)$$

Here $P(n,t)$ is the probability that the diffusing nucleus experiences exactly n encounters during time t. It is to be noted that the topology of the diffusion process, reflected in the $P(n,t)$, and the dynamics of the NN interaction, reflected in the f_α, contribute to the relaxation process in a separable way. $P(n,t)$ is decomposed as

$$P(n,t) = \sum_{M=n}^{\infty} P(n,M)\rho(M,t) \quad (5.10)$$

where, if Z is the cation NN coordination,

$$P(n,M) = (Zc)^n(1-Zc)^{M-n}\frac{M!}{n!(M-n)!} \quad (5.11)$$

is a binomial distribution representing the probability that n out of M fluorine ions are NN to Mn ions. The factor

$$\rho(M,t) = \frac{(Wt)^M e^{-Wt}}{M!} \quad (5.12)$$

is a Poisson distribution for the probability that the F^-, hopping at rate W, executes M jumps in time t. The above choices yield a simple exponential form for the relaxation function, $F_\alpha(t) = e^{-t/T_\alpha}$ with

$$\frac{1}{T_\alpha} = (1-f_\alpha)ZcW . \quad (5.13)$$

Equation (5.11) is a probabilistic description appropriate to a *static* random distribution of F^- ions on the vacant sc sublattice and a concentration c of Mn^{2+} ions substitutionally introduced for the Pb^{2+} ions in PbF_2. This approximation is too simplistic, as it neglects both the particles' history and the influence of the lattice topology on the F^- diffusion. Suppose we follow the diffusion of a given F^- ion that is not NN to a Mn^{2+} as it moves through the crystal, by discrete NN jumps on the sc anion sublattice. Initially, it has four cation NN and on its first jump retains two former and acquires two *new* cations as NN. Thus, it has a probability $Zc/2$, rather than Zc, of encountering a Mn^{2+} on the first jump. Such memory effects persist. The second jump, for example, may be to the initially occupied site with the certainty of *no* new encounters with a Mn^{2+} spin there. This is to be contrasted with the assumptions implicit in the AEM, where the F^- has a probability equal to Zc of encountering a Mn^{2+} on every jump, as would be the case only if it traversed large distances $d >> a_0$ on each move.

B. Impact model

We present an analysis which avoids both the statistical inadequacies just discussed and the unwarranted dynamical approximation of the AEM. As in the AEM (or in the problems of pressure broadening in dilute gases, electron scattering by dilute impurities in metals, or μSR—the positive muon spin relaxation in solids), we recognize that the random process occurs by a succession of collisions with dynamically uncorrelated objects (here, the Mn^{2+} spins). The duration of each collision, of the order of the F^- hopping time, is very short compared to the relaxation times T_1 and T_2 of the macroscopic nuclear magnetization. The "impact theory limit," in which only the net effect of each total collision is important, rather than the time dependence of events during a collision,

again allows us (as in the AEM) to factor the relaxation process into a term describing the effect of the interaction of a ^{19}F spin I with a single Mn^{2+} spin S and one describing the F^- ion motion. With regard to the latter, explicit recognition must be taken of the fact that the eight NN F^- ion positions surrounding a Mn^{2+} ion constitute an "active cell" at which nuclear relaxation occurs. Therefore, we take as the encounter time τ_l of Eq. (5.5) *not* the residence time at a single active site, but rather the interval during which the F^- ion remains in an active cell (including those brief escapes and returns from the cell which take place in times short compared with the electron-spin-relaxation time τ_{sl}). Then, if the *average* result of a single encounter by a F^- ion on its nuclear spin I_α can be expressed as

$$\langle I_\alpha^{\text{after}} \rangle = \phi_\alpha I_\alpha^{\text{before}} \tag{5.14}$$

(a result to be demonstrated later in this section), it follows that the *total* nuclear magnetization $M_\alpha(t)$ will be given, in general, by

$$M_\alpha(t) = \sum_{n=0}^{\infty} P_n(t)\phi_\alpha^n M_\alpha(0) \ . \tag{5.15}$$

Here $P_n(t)$ is the probability for a single F^- ion to have exactly n encounters in time t. As the Mn^{2+} ions are distributed at random, and their concentration is small, $P_n(t)$ can be taken to have a Poisson distribution

$$P_n(t) = \frac{(Rt)^n}{n!} e^{-Rt} \ , \tag{5.16}$$

where R is the average encounter rate. Then Eq. (5.15) can be summed to give

$$M_\alpha(t)/M_\alpha(0) = e^{-t/T_\alpha} \ ,$$

where

$$\frac{1}{T_\alpha} = R(1-\phi_\alpha) \ . \tag{5.17}$$

Note that this result has the same structure as the AEM prediction, Eq. (5.13). However, in the AEM, $R = ZcW$ is the rate of encountering active *sites* and $\langle f \rangle$ is the average relaxation at such a site, whereas in our model R is the rate at which the active *cells* are visited and ϕ represents the average relaxation that is produced as a result of the total time spent within that cell. We will find important modifications in both R and ϕ_α from what is found from the AEM. We first consider the encounter rate R.

The calculation of R proceeds as if the F^- ions move on an empty lattice, although the real situation corresponds to motion on an almost filled one. As regards the gross motion of the F^- ions, if there is no important cooperative motion (as there may, in fact, be at the highest temperatures[8]) the two are the same. Let us assume that vacancy hopping dominates the F^- ion motion. When the vacancy fraction $v \ll 1$, vacancy hopping occurs on a time scale much shorter than that which characterizes the bulk ion diffusion, the two differing by the ratio v. Those correlated motions of a F^- ion which take place during the passage of a single vacancy occur on the *short* time scale of the vacancy hopping and their contribution to nuclear relaxation is very small. The remaining F^- ion motion is what one would find in the hypothetical empty lattice, but with a rate W reduced by a factor v from the vacancy hopping rate. Experimentally, W is determined from conductivity measurements,[7,22] once v is known.

Consider the motion of a F^- ion which is at the origin at $t=0$. We denote the position of a particular active site by the lattice vector $\vec{T}_i$. If $F_l(\vec{T}_i)$ is the probability that the F^- ion reaches $\vec{T}_i$ on the lth step and has seen no active sites in the previous $l-1$ hops, we then need the average encounter rate

$$R \equiv \frac{1}{t}\left\langle \sum_{l=1}^{N(t)} \sum_i F_l(\vec{T}_i) \right\rangle \ , \tag{5.18}$$

where $N(t)$ is the number of steps in time t and the average is taken over Mn configurations. We can abstract the required sum in Eq. (5.18) by first relating the F_l to the familiar random walk probability $P_n(\vec{T}_j)$ of finding the F^- ion at $\vec{T}_j$ in the nth step, by the self-evident equation

$$P_n(\vec{T}_j) = \sum_{l=1}^{n} \sum_i F_l(\vec{T}_i) P_{n-l}(\vec{T}_j - \vec{T}_i) \ , \tag{5.19}$$

where i is to be summed over all active sites. It follows directly that

$$\sum_j \sum_{n=1}^{N} P_n(\vec{T}_j) = \sum_{i,j} \sum_{k=0}^{N-1} P_k(\vec{T}_j - \vec{T}_i) \sum_{l=1}^{N-k} F_l(\vec{T}_i) \ . \tag{5.20}$$

For low concentrations, $c \ll 1$, the desired sum over the F_l can be factored approximately from the right-hand side of Eq. (5.20). The sum over i on the right-hand side is dominated by the eight terms in which $\vec{T}_i$ and $\vec{T}_j$ are associated with the *same* Mn, because the P_k fall off rapidly with distance. If we keep only these eight terms, the sum over i is independent of the concentration c of impurities. Furthermore, for the calculation of R, we are interested in the large N limit of the sum over F_l. Hence, since $P_k(\vec{T}_j - \vec{T}_i)$ also falls off rapidly with k, we can take $N-k \simeq N$ in the upper limit of the sum, and then

$$\sum_j \sum_{l=1}^{N} F_l(\vec{T}_j) \simeq \frac{\sum_j \sum_{n=1}^{N} P_n(\vec{T}_j)}{\sum_{\vec{\Delta}} \sum_{k=0}^{N-1} P_k(\vec{\Delta})} \ , \tag{5.21}$$

where $\vec{\Delta}$ denotes one of the eight vectors which connect one corner of the active cube with the others or to itself. Again, since N is large and $P_k(\vec{\Delta})$ falls rap-

idly with increasing k, we can let $N \to \infty$ in the denominator, which is then the sum over $\vec{\Delta}$ of the appropriate simple cubic lattice Green's functions

$$u = \sum_{\vec{\Delta}} \sum_{k=0}^{\infty} P_k(\vec{\Delta}) = \sum_{\vec{\Delta}} \int \frac{d^3q}{(2\pi)^3} \frac{e^{i\vec{q}\cdot\vec{\Delta}}}{1-\gamma_q} \quad , \tag{5.22}$$

where

$$3\gamma_q = \cos q_x a_0 + \cos q_y a_0 + \cos q_z a_0 \quad .$$

Finally then, we obtain

$$R \simeq \frac{1}{ut}\left\langle \sum_j \sum_{n=1}^{N} P_n(\vec{T}_j) \right\rangle \simeq \frac{ZcW}{u} \quad , \tag{5.23}$$

where Z is the cation coordination number with respect to a F^- site ($Z=4$ in PbF_2) and we have taken $N(t) = Wt$ at long times.

We see that the geometry of the lattice enters R through the coordination number Z and the factor u which describes the effects of paths which begin and end on the cluster of sites which constitute an active cell. For the simple cubic F^- lattice the sum over lattice Green's functions u equals 4.32, so $Z/u \simeq 0.93$. The corrections to R are of higher orders in concentration and hence are much smaller. The result Eq. (5.23) reveals an interesting fact. On the average, the diffusing F^- ions encounter approximately only one new cation NN per hop. This anticipated result is in keeping with the qualitative discussion of the F^- ion diffusion presented in the beginning of this section.

A computer simulation corroborated the analytical approach given above. A $32 \times 32 \times 32$ sc lattice was used, with periodic boundary conditions applied. The cation sites were decorated with a fraction c of Mn^{2+} spins randomly substituted for the Pb^{2+} ions. A F^- ion was placed at random on the sc lattice and its walk was followed. From repeated trials, $P(0,m)$, the probability that no encounter with a Mn^{2+} spin would occur in m steps was found to decay exponentially with m, corresponding to an encounter rate $R = 1.06cW \simeq ZcW/4$, for cm between 0 and approximately 7.

We now turn to the dynamics and the calculation of ϕ, the factor in the relaxation rate which describes the *average* relaxation in one encounter. If the relaxation for a specific residence time t in the active cell is $\phi(t)$, then ϕ is

$$\phi = \int_0^{\infty} P_{\rm res}(t)\,\phi(t)\,dt \quad , \tag{5.24}$$

where $P_{\rm res}(t)$ is the probability distribution for residence times. The rate of escape of F^- ions from the active sites is approximately $W/2$ because, in a single hop, the F^- has only a 50% chance of hopping to an inactive site. Paths which leave the cell and subsequently return to it only contribute a small correction, the leading term of which is $\frac{1}{12}$. Hence, summing over the probability $\rho(n,t)$ of having exactly n hops in time t [see Eq. (5.12)], we have

$$P_{\rm res}(t) \simeq \frac{W}{2} \sum_{n=0}^{\infty} (2)^{-n} \rho(n,t)$$

$$\equiv (W/2)\exp(-Wt/2) \quad . \tag{5.25}$$

It remains to calculate explicitly the relaxation function,

$$\phi_\alpha(t) \equiv \langle I_\alpha(t) I_\alpha^\dagger(0)\rangle / \langle I_\alpha(0) I_\alpha^\dagger(0)\rangle \quad . \tag{5.26}$$

The time dependence of $I_\alpha(t)$, apart from a trivial dependence given by the nuclear Larmor precession ω_0, is determined by the hyperfine interaction with the Mn^{2+} spin $\vec{S}$. A perturbative approach, at first glance, would not appear to be unreasonable; the effect of any one encounter on the *total* nuclear magnetization, whose relaxation is being studied, is small. However, in order to incorporate the F^- ion motion into a theory of nuclear magnetization correlation functions, the schemes so far devised (both in Ref. 11 and in the present work) require one to describe the time evolution of the *individual* nuclear spin and not the total magnetization. Perturbation theory breaks down for the single-spin dynamics whenever $|A\tau_c| > 1$, where A is a measured of hfs interaction and τ_c is the duration of an encounter or the electron-spin correlation time, whichever is shorter. The linear equation (5.2) has the formal solution[13]

$$I_\alpha(t) = T\exp\left[i\int_0^t dt'\,\mathcal{K}'(t')^x\right] I_\alpha(0) \quad , \tag{5.27}$$

where T is the usual operator which time orders the exponential and $a^x b \equiv [a,b]$. The double average over electron spin and spatial coordinates of the time ordered exponential can be expressed as the exponential of a sum of cumulant averages. If the hyperfine perturbation represents a Gaussian random process, all cumulant averages beyond the second vanish identically. In this case, Eq. (5.3) is a suitable approximation independent of the magnitude of $|A\tau_c|$. However, electron-spin fluctuations (produced by spin-lattice or spin-spin interactions) and F^- diffusion give rise to *Poisson,* rather than Gaussian, modulation of the interaction. Therefore, the validity of Eq. (5.3), in the AEM, relies on the smallness of $|A\tau_c|$. However, $|A\tau_c|$ can be large at low temperatures where both conditions for the validity of Eq. (5.3) are therefore violated.

Let us then consider explicitly the time dependence of $I_\alpha(t)$ in the region where the electronic Larmor frequency $\omega_e \gg W$, the F^- ion hopping rate, which is the case at all but the highest temperatures in PbF_2 in all of our experiments. In this instance the transverse fluctuations of $\vec{S}$ have little effect, on the average, on $I_\alpha(t)$ and the effective hyperfine Hamil-

tonian becomes

$$\mathcal{H}'(t) = \sum_\alpha I_\alpha A_{\alpha z} S_z(t) \ . \tag{5.28}$$

As a consequence of electronic-spin relaxation, S_z fluctuates between its $2S+1$ values at a rate $\nu \equiv (\tau_{sl})^{-1}$. In an interval τ_1 during which S_z retains a particular value m_1, the total effective Hamiltonian determining $I_\alpha(t)$ is

$$\mathcal{H}(m_1) = -\gamma \vec{I} \cdot \vec{H}_e(m_1) \ , \tag{5.29}$$

where

$$\vec{H}_e(m_1) = H_0 \hat{z} + \frac{m_1}{\gamma} \sum_\alpha A_{\alpha z} \hat{\alpha} \tag{5.30}$$

is the instantaneous effective field about which $\vec{I}$ precesses when $S_z = m_1$. It follows that

$$\vec{I}(t_1+\tau_1) = \exp[-i\gamma\tau_1 \vec{I}\cdot\vec{H}_e(m_1)]\vec{I}(t_1) \times \exp[i\gamma\tau_1 \vec{I}\cdot\vec{H}_e(m_1)] \ , \tag{5.31}$$

if S_z takes the value m_1 between times t_1 and $t_1+\tau_1$. In general this would admix *different* components of $\vec{I}$. However, if $\vec{H}_e$ has reflection symmetry normal to $\hat{z}$ then, when the average is taken over the eight sites in an active cell, the mixing vanishes. Thus,

$$I_\alpha(t_1) = g_\alpha(m_1,t_1) I_\alpha(0) \ , \tag{5.32}$$

where

$$g_z(m,t) = [H_{ez}^2 + (H_{ex}^2 + H_{ey}^2)\cos(\gamma H_e t)]/H_e^2 \ ,$$
$$g_\pm(m,t) = \exp[\mp i\gamma(H_{ez} - H_0)t] \ . \tag{5.33}$$

The m dependence of H_e is explicitly given in Eq. (5.30).

A full encounter of duration t consists of a sequence of $(n-1)$ changes in the value of S_z at times $0 \leq t_1 < t_2 \cdots < t_{n-1} \leq t$. The probability that changes occur only at t_1 within dt_1, at t_2 within dt_2, etc., is clearly

$$(\nu e^{-\nu t_1})(\nu e^{-\nu(t_2-t_1)}) \cdots (\nu e^{-\nu(t_{n-2}-t_{n-1})}) e^{-\nu(t-t_{n-1})} dt_1 \cdots dt_{n-1} = \nu^{n-1} e^{-\nu t} dt_1 \cdots dt_{n-1} \ ,$$

where $\nu \equiv \tau_{sl}^{-1}$. Thus the average over all possible sequences within the time t gives

$$\langle I_\alpha(t)\rangle = \sum_{n=1}^{\infty} \nu^{n-1} e^{-\nu t} \int_0^t dt_{n-1} \int_0^{t_{n-1}} dt_{n-2} \cdots \int_0^{t_2} dt_1 \, g_\alpha(m_n, t-t_{n-1}) g_\alpha(m_{n-1}, t_{n-1}-t_{n-2}) \cdots g_\alpha(m_1,t_1) I_\alpha(0) \ . \tag{5.34}$$

Finally, the average over encounter times t of Eq. (5.24) yields for the average single encounter relaxation

$$\phi_\alpha = \frac{W}{2} \sum_{n=1}^{\infty} \nu^{n-1} \prod_{j=1}^{n} \tilde{g}_\alpha\left(m_j, \frac{W}{2}+\nu\right) \ , \tag{5.35}$$

where $\tilde{g}$ indicates the Laplace transform of g. If the value that m_j assumes in any one interval is uncorrelated with the value it has in any other, then we may approximate the product $\prod \tilde{g}_\alpha(m, W/2+\nu)$ by $\langle \tilde{g}_\alpha \rangle^n$, where $\langle \tilde{g}_\alpha \rangle$ is the average over all m of $\tilde{g}_\alpha(m, W/2+\nu)$ obtained from the Laplace transform of Eq. (5.33)

$$\langle \tilde{g}_z(s)\rangle = \frac{1}{s}\left[1 - \frac{1}{2S+1}\sum_m \gamma^2 \frac{(H_{ex}^2 + H_{ey}^2)}{s^2 + (\gamma H_e)^2}\right] \ ,$$

and

$$\langle \tilde{g}_\pm(s)\rangle = \frac{1}{2S+1}\sum_m \frac{s}{s^2 + (mA_{zz})^2} \ , \tag{5.36}$$

at $s = W/2+\nu$. Note that the components of $\vec{H}_e$, through $\tilde{A}$, depend on the angle between $\vec{H}_0$ and the Mn^{2+}–F^- bond axis ($\hat{Z}$); averages over the directions of $\vec{H}_0$ with respect to $\hat{Z}$ are implicit here and are explicitly shown in Eq. (A2) of the Appendix.

The now geometric sequence in Eq. (5.35) can be summed explicitly, to give

$$\phi_\alpha = \frac{W\langle \tilde{g}_\alpha\rangle}{2(1-\nu\langle \tilde{g}_\alpha\rangle)} \ . \tag{5.37}$$

Substituting this and the result (5.23) for the rate R into Eq. (5.17), we obtain the final results for the relaxation rates

$$\frac{1}{T_\alpha} = \frac{ZcW}{u}\left[1 - \frac{W\langle \tilde{g}_\alpha(W/2+\nu)\rangle/2}{1-\nu\langle \tilde{g}_\alpha(W/2+\nu)\rangle}\right] \ , \tag{5.38}$$

where we recall $Z/u \approx 1$ for the PbF_2 lattice, W is the hopping rate, c the impurity concentration, and ν the electronic spin-lattice relaxation rate; the relaxation functions $\langle \tilde{g}\rangle$ are given by Eq. (5.36).

These impact model results remain valid over a wide range of parameters, but they do break down if transverse electronic spin fluctuations begin to contribute appreciably to the nuclear relaxation. Then the time development of $I(t)$ can no longer be represented as finite rotations about a discrete sequence of static effective fields [and $\langle I_\alpha(t)\rangle$ will depend, in general, upon *all* components of $\langle \vec{I}(0)\rangle$ rather than just on $\langle I_\alpha(0)\rangle$].

The transverse spin fluctuations become important when they develop substantial spectral weight at low frequencies ($\lesssim \omega_0$), i.e., when the larger of the spin-

lattice rate ν and the hopping rate W becomes at least of the order of the electronic Larmor frequency ω_e: $\omega_e\tau_c \lesssim 1$, where the correlation time τ_c is the smaller of ν^{-1} and W^{-1}. But small τ_c is the requirement for the rapid convergence of perturbation theory, which is an expansion in $A\tau_c$, where A is a measure of the hyperfine interaction strength. Thus, if $A < \omega_e$, the perturbation expansion will become useful before the impact model approximation breaks down. In Mn:PbF_2 at a field where the nuclear frequency $\omega_0/2\pi = 10$ MHz, we have $\omega_e \simeq 10^{11}$ rad/sec, whereas $A \sim 10^8$ sec^{-1} $\ll \omega_e$. At low temperatures hopping is slow, and τ_c is set by the electronic spin-lattice relaxation rate ν. In the present system ν, which is only weakly temperature dependent, in comparison with W, is of the order of 10^8–10^9 sec^{-1}, so $\omega_e/\nu \gg 1$, and the transverse fluctuation effects which invalidate the impact model approximation enter only at temperatures sufficiently high that the hopping rate W becomes of the order of ω_e ($\sim$800 K in Mn:PbF_2). Also, A/ν is of order unity. In fact, if A/ν were $\ll 1$, then perturbation theory would be valid everywhere, so the only case of interest is $A \gtrsim \nu$, where the criterion for convergence of the perturbation expansion becomes $A/W \ll 1$. Then in this limit, but with $W \ll \omega_e$ so that the impact results remain valid, we have from Eqs. (5.36) and (5.37)

$$\phi_z \simeq 1 - \frac{16S(S+1)\langle A_{10}^2\rangle}{3W^2(1+2\nu/W)} ,$$
$$\phi_+ \simeq 1 - \frac{4S(S+1)\langle A_{zz}^2\rangle}{3W^2} \qquad (5.39)$$
$$(\nu, A_{\alpha\beta} \ll W \ll \omega_e) ,$$

where the angular average of the hyperfine tensor components $\langle A_{\alpha\beta}^2\rangle$ is defined in Eq. (A2) of the Appendix. We compare these results with those of perturbation theory as obtained from Eqs. (5.3)–(5.8), with $W/2$ instead of W properly used in Eq. (5.8) for the distribution in residence times in an active cell:

$$f_z \simeq 1 - \frac{16S(S+1)\langle A_{10}^2\rangle}{3W^2(1+2\nu/W)} - \frac{32S(S+1)(\langle A_{1-1}^2\rangle + \langle A_{11}^2\rangle)}{3(W^2+4\omega_e^2)} ,$$
$$f_+ \simeq 1 - \frac{4S(S+1)\langle A_{zz}^2\rangle}{3W^2} - \frac{8S(S+1)\langle A_{10}^2\rangle}{3W^2\left(1+\frac{2\nu}{W}\right)} - \frac{16S(S+1)(\langle A_{1-1}^2\rangle + \langle A_{11}\rangle^2)}{3(W^2+4\omega_e^2)} . \qquad (5.40)$$

In obtaining Eqs. (5.40) we have assumed ω_0, ν, $A_{\alpha\beta} \ll W$ and $\omega_0 \ll \nu \ll \omega_e$. In the limit that $W \ll \omega_e$, the final term in each equation of (5.40) makes a negligible contribution to the relaxation. Thus, the expressions for ϕ_z [Eq. (5.39)] and f_z [Eq. (5.40)] are identical in this limit. The expression for f_+ reduces to that for ϕ_+ if the term proportional to $\langle A_{10}^2\rangle$ in Eq. (5.40) is neglected. This contribution arises from the nonsecular interaction which is not included in the impact approximation. The perturbation expansion is useful over a broader range of the parameters than is imposed by the restrictions above. The general results, which are algebraically complex, can be found in Ref. 5. Those expressions were, in fact, used for the numerical results reported below. From the simpler form (5.40), though, we can immediately see the source of the high-temperature peak in $T_1^{-1} = R(1-f_+)$: the final term gives a contribution proportional to $W/(W^2+4\omega_e^2)$.

VI. MODEL PREDICTIONS AND COMPARISON WITH EXPERIMENTAL RESULTS

A. Model predictions

The model predictions for T_1 and T_2, in addition to the T and H_0 dependence, are parametric functions of $\tilde{A}$ and τ_{sl}. The ^{19}F hfs tensor, referred to the bond axis joining the F^- and Mn^{2+} ions, is expressible in terms of symmetric A_s and asymmetric A_p components. These relations are given in the Appendix. A_s and A_p for Mn:PbF_2 have been determined from a single-crystal, NMR study at low temperatures ($T \simeq 1.3$ K) of ^{19}F NN to Mn^{2+}; $A_s = 33.82$ and $A_p = 7.82$ MHz.[23] In general, A_s and A_p are expected to be temperature dependent, as they depend on overlap and electron transfer effects and could vary with T because of both the harmonicity and anharmonicity of the lattice vibrations. For example, in Mn:$KMgF_3$ A decreases by 25% as the temperature is increased from 300 to 1000 K.[24] Considering the large anharmonicity of PbF_2, one might expect the T dependence of $\tilde{A}$ to be larger still. Hence the low T (1.3 K) values for A_s and A_p quoted above are to be regarded as *upper* bounds on what the high-T values might be.

No direct experimental determination of τ_{sl} vs T for Mn^{2+} in PbF_2 has been made. Nevertheless, a lower bound on τ_{sl} may be set using the measured T dependence of the Mn^{2+} EPR linewidth in Mn:PbF_2.[10] If the broadening of the EPR resonance observed above 600 K is caused by electronic spin-lattice relaxation, then a lower limit may be placed on τ_{sl} at 600 K of 2×10^{-9} sec. The EPR data are insuffi-

cient to establish τ_{sl} vs T above 600 K, but the measurements indicate that τ_{sl} continues to decrease with increasing T.

With the above bounds in mind, we first examine the τ_{sl}, H_0, and $\tilde{A}$ dependence of the impact model calculations before making a "best fit" comparison with the experimental observations. As we have discussed, this is an appropriate theory below temperatures ($\sim$700 K in this system for $\omega_0/2\pi \simeq 50$ MHz) at which transverse (S_x and S_y) spin fluctuations contribute appreciably to the nuclear T_1. Near the upper end of that temperature range the perturbation expansion is already useful and agrees with the impact theory; at higher T we will later use perturbation theory in order to include the important effects of transverse electron-spin fluctuations and to make comparison with experiment.

The temperature dependence in the theory enters dominantly through that of the parameters. We have taken all except W to be approximately constant, since their dependence on T is not well known but is much weaker than that of W. We have chosen to extract the values of $W(T)$ from measurements[7,22] of the dc ionic conductivity in PbF_2, as was also done in Ref. 8, rather than to use some theoretical model (e.g., thermally activated behavior.)

In Fig. 6 the τ_{sl} dependence of $T_1^{-1}(T)$ is shown for the following values of the parameters: $A_s = 34$ MHz, $A_p = 6$ MHz, $H_0 = 21.75$ kOe. With τ_{sl} varying from 10^{-7} to 10^{-10} sec, the calculations encompass the region between $\omega_0\tau_{sl} > 1$ and $\omega_0\tau_{sl} < 1$. The general trend is seen to be a broadening of the peak and a reduction in the high-temperature T_1^{-1} as τ_{sl} is decreased. In the low-T region, $W\tau_{sl} << 1$, relaxation is most effective when the local field fluctuations experienced during the encounter occur at a rate comparable with ω_0, i.e., $\omega_0\tau_{sl} = 1$. This will occur when $\tau_{sl} \simeq 2 \times 10^{-9}$ sec. In the opposite extreme, appropriate to high temperatures, where many Mn^{2+} encounters are required to relax the nucleus, one expects, and finds, negligible τ_{sl} dependence to T_1 provided that $W\tau_{sl} >> 1$. Only in the case where $W\tau_{sl} \lesssim 1$, for all T, is the τ_{sl} dependence of T_1 evident at the highest temperatures.

The τ_{sl} dependence of $T_2^{-1}(T)$ is illustrated in Fig. 7 for the same values of the parameters A_s, A_p, and H_0 used in Fig. 6 but τ_{sl} now varies between 10^{-8} and 10^{-10} sec. In contrast to the T_1 process, the dominant T_2 process does not require S_z fluctuations and therefore electron spin relaxation acts to reduce the nuclear T_2^{-1} at all τ_{sl} for which $A_s\tau_{sl} \lesssim 1$. Hence, as τ_{sl} is decreased, T_2^{-1} decreases throughout the temperature region.

The field dependence of $T_1^{-1}(T)$ is shown in Fig. 8 for $A_s = 34$ MHz, $A_p = 6$ MHz, and $\tau_{sl} = 2 \times 10^{-9}$ sec. For H_0 below $A_{zz}S/\gamma \simeq 21$ kOe ($\omega_0/2\pi = 85$ MHz), T_1 is essentially independent of H_0, but a pronounced H_0 dependence is predicted for larger ap-

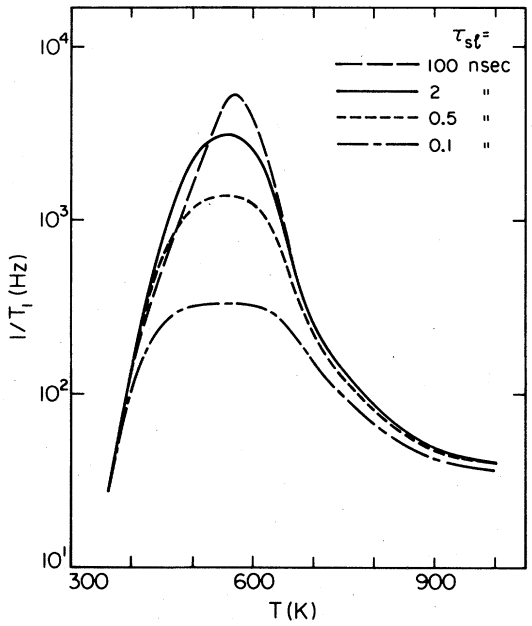

FIG. 6. Impact model predictions for T_1^{-1} vs T at $\omega_0/2\pi = 87$ MHz, as a function of τ_{sl}. Each value of τ_{sl} is assumed to be temperature independent. The values of the ^{19}F hfs interaction were chosen to be $A_s = 34$ MHz, $A_p = 6$ MHz, and $c = 0.017\%$. Both the shape of the T_1^{-1} peak and its magnitude display a marked τ_{sl} dependence. For T below 500 K, the maximum T_1^{-1} occurs when $\omega_0\tau_{sl} \simeq 1$, which implies $\tau_{sl} = 2 \times 10^{-9}$ sec. T_1^{-1} is reduced from this value in both extremes, i.e., $\omega_0\tau_{sl} >> 1$ and $\omega_0\tau_{sl} << 1$.

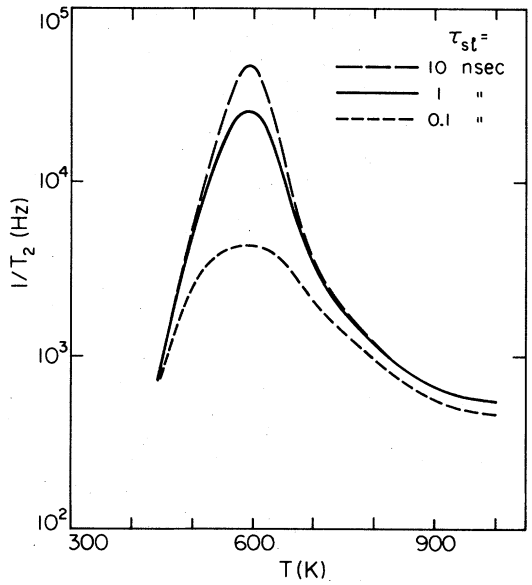

FIG. 7. Impact model calculations for T_2^{-1} vs T as a function of τ_{sl} for the same values of ω_0, A_s, A_p, and c given in the Fig. 6 caption. T_2^{-1} exhibits a τ_{sl} dependence only when $A_s\tau_{sl} < 1$ and decreases with decreasing τ_{sl}.

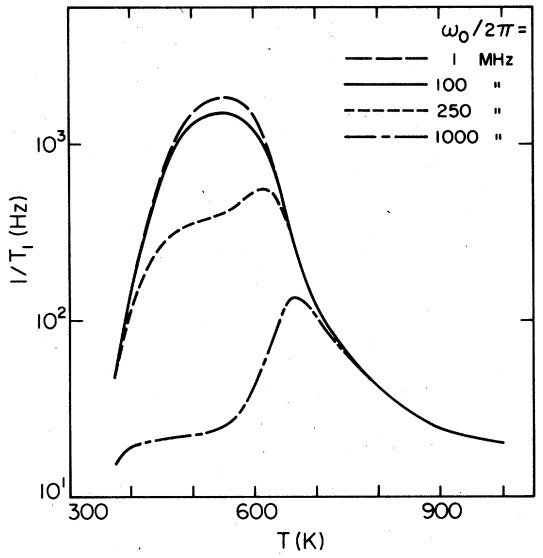

FIG. 8. Impact model calculations for T_1^{-1} vs T for several values of $\omega_0/2\pi$ (MHz) $=4.0H_0$ (kOe) for the same values of A_s, A_p, and c given in the Fig. 6 caption. T_1^{-1} exhibits a non-negligible H_0 dependence only for fields such that $H_0 > (1/\gamma)A_{zz}S$. In this case, a peak in T_1^{-1} occurs when the ion hopping rate $W \simeq \omega_0$.

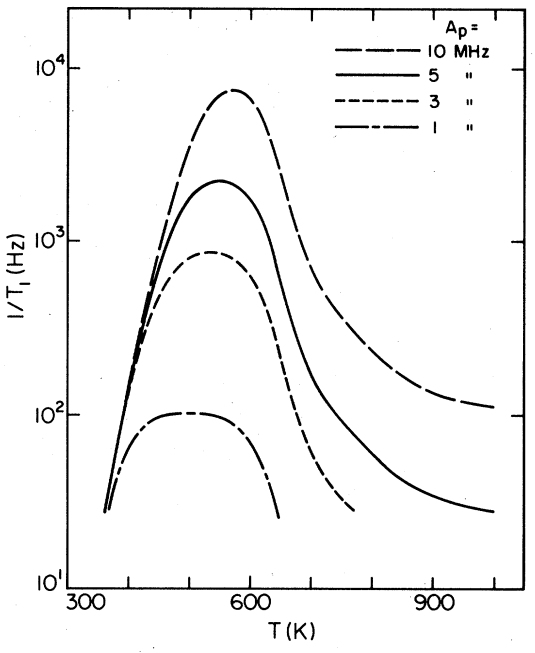

FIG. 9. Impact model predictions for T_1^{-1} vs T as a function of A_p. The same values of ω_0, A_s, and c were used as are given in the caption of Fig. 6. At temperatures above the peak ($T > 700$ K), $T_1^{-1} \propto A_p^2 S(S+1)\,\tau_c$ while in the low-T limit $T_1^{-1} \propto c/\tau_c$, independent of A_p. Therefore the peak value of T_1^{-1} grows and occurs at larger T with increasing A_p.

plied fields. For $H_0 \geq 62.5$ kOe ($\omega_0/2\pi = 250$ MHz), T_1^{-1} is reduced from its low field value and a second peak is predicted. The peak occurs at higher T for larger H_0. The transition from a low field, H_0 independent T_1 to a high field, H_0 dependent T_1 is the most striking prediction of the impact model, and may be understood as follows: During the encounter, the ^{19}F nucleus experiences a total $\hat{z}$ directed field $H_z = H_0 + (1/\gamma)A_{zz}S_z$ and a transverse field $H_\perp = (1/\gamma)S_z\,(A_{zx}\hat{x} + A_{zy}\hat{y})$. (For the present we disregard fields arising from S_x and S_y.) As S_z fluctuates, it either augments or reduces the total $\hat{z}$ field at the nucleus. For the particular values of H_0 and S_z such that $(1/\gamma)A_{zz}S_z = -H_0$ there can be a complete cancellation of the z directed field while the transverse field $H_\perp \neq 0$. If this situation obtains, complete relaxation of the nucleus will occur. Clearly this is a special case. However appreciable cancellation will occur for any $H_0 \leq (1/\gamma)A_{zz}S$. Indeed T_1 is essentially field independent for all H_0 that satisfy the above condition.

In the opposite limit, $H_0 > (1/\gamma)A_{zz}S$, this mechanism breaks down and T_1 becomes a function of H_0. In this case, where relaxation during a single encounter is an improbable event, the largest relaxation rate occurs when the rate of the local field modulation is of order ω_0. When $\omega_0\tau_{sl} >> 1$, this occurs for $\omega_0 \simeq W$ and T_1^{-1} will have a peak, which moves towards higher T (larger W) the larger H_0 is.

The dependence of $T_1^{-1}(T)$ on the magnitude of A_p is illustrated in Fig. 9 for $A_s = 34$ MHz, $\tau_{sl} = 2 \times 10^{-9}$ sec, and $H_0 = 21.75$ kOe. The effect of decreasing A_p is to reduce the T_1^{-1} throughout the whole of the temperature range. As $A_s > A_p$, varying A_p does little to affect the total z directed field experienced during an encounter but the A_p term is the sole source of the transverse fields which produce the NMR relaxation. Hence T_1^{-1} grows as A_p increases.

B. Comparison with experiment

In Fig. 10 "best fit" impact model calculations for T_2^{-1} are compared with the experimental results obtained in sample C. The best agreement is obtained using the values $A_s = 34$ MHz, $A_p = 6$ MHz, $\tau_{sl} = 2 \times 10^{-9}$ sec, and $c = 0.017$ mole%, which are to be compared with the experimentally determined values ($A_s = 33.82$ MHz and $A_p = 7.82$ MHz at low T, and $c = 0.015 \pm 0.005$ mole%). For temperatures below 650 K, the model calculation reproduces the observed behavior, but at higher temperatures the value predicted for T_2^{-1} falls well below the measured relaxation rate. (We remind the reader that the initial T_2 below $T = 400$ K is dominated by the effects of F-F

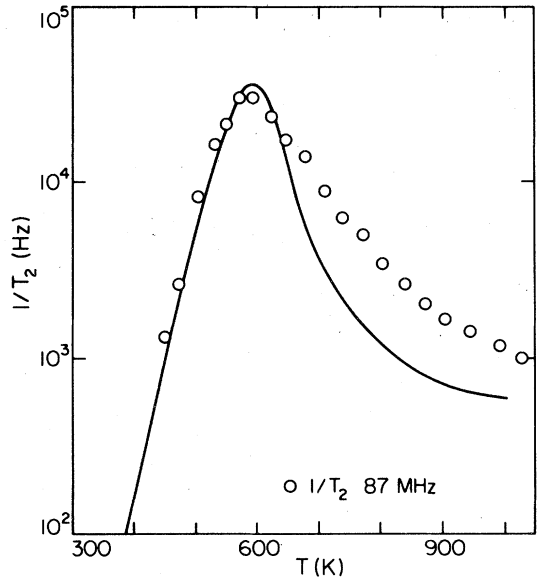

FIG. 10. Comparison of impact model calculations for T_2^{-1} vs T with the experimental results obtained on sample C at a frequency $\omega_0/2\pi = 87.17$ MHz. The parameter values chosen to obtain this "best agreement" were $A_s = 34$ MHz, $A_p = 6$ MHz, and $\tau_{sl} = 2 \times 10^{-9}$ sec. The model predicts both the magnitude and position of the T_2^{-1} peak but at higher temperatures it seriously underestimates the observed T_2^{-1}.

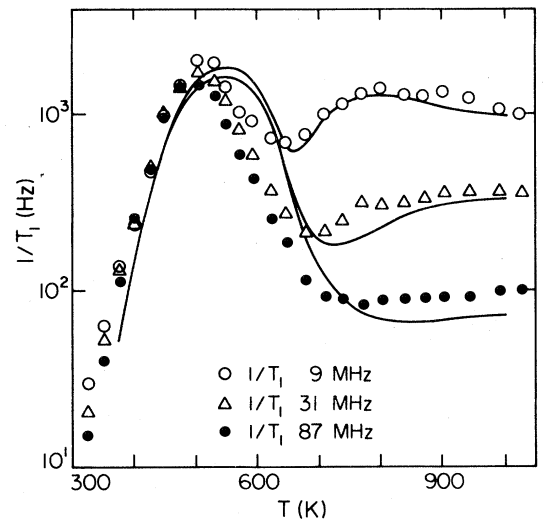

FIG. 11. Comparison of the calculations for T_1^{-1} vs T with the experimental results obtained in sample C at three different frequencies. The parameter values are the same as those given in the Fig. 10 caption. The model predicts both the magnitude and ω_0 dependence of the measured T dependence of T_1^{-1}. For T below 650 K it confirms the appropriate lack of ω_0 dependence observed but the position of the peak is at a higher T than is found experimentally. The quantitative agreement found for T above 650 K is to be contrasted with that shown in Fig. 10 for T_2^{-1} in the same temperature region.

dipole interactions; the current discussion deals only with the additional relaxation associated with the hyperfine interactions, so the low-temperature points of Fig. 3 are not displayed in Fig. 10.)

In contrast to the above result, model calculations for the T_1 for this sample compare favorably with the measured relaxation rates even at the highest temperature investigated. This is illustrated in Fig. 11 where the predicted ω_0 dependence of T_1 vs T, using the same parameter values as Fig. 10, is compared to the relaxation rates in sample C. The source of the low-temperature T_1^{-1} peak is the previously described impact mechanism and a major triumph of the model is that it predicts the appropriate lack of ω_0 dependence to T_1 in this region. The high-temperature peak is produced by coupling of the nuclei to the transverse fluctuation in S, which is important only when $W \gtrsim \omega_e$, where the impact approximation is no longer valid, but where we have shown that perturbation theory applies. The predicted position of the low-temperature peak occurs at higher T than is observed.

A comparison of the theoretical predictions for the frequency dependence of $T_1^{-1}(T)$ in the impact model with those of a *corrected* perturbation theory is shown in Fig. 12. Only the longitudinal fluctuations

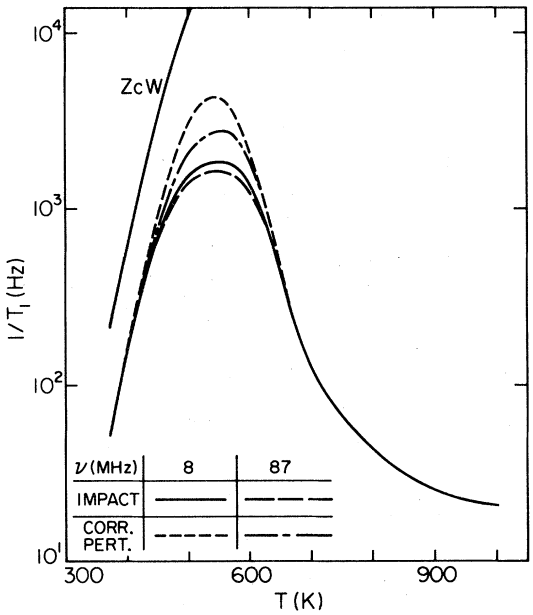

FIG. 12. Comparison between the impact model and "corrected" perturbation calculations for T_1^{-1} vs T at two frequencies. The models are equivalent in both temperature extremes but differ significantly in the region between 400 and 700 K. The "corrected" perturbation results have a more pronounced frequency dependence and a larger relaxation rate in this temperature range. The low-temperature part of the AEM predictions is also shown in the figure as the curve labeled *ZcW*.

in S_z are considered; hence the high-temperature peak, caused by the transverse fluctuations, is absent. Note that both the magnitude of T_1^{-1} and, more significantly, its frequency dependence is smaller in the impact model than it is in the *corrected* perturbation theory. By *"corrected"* we mean that proper account is taken of the statistical character of the F^- ion motion. In the AEM, where this is not done, the low-temperature T_1^{-1} behavior is given by ZcW, as is shown in Fig. 12. The impact model results are in better agreement with experiment than those obtained from the *corrected* perturbation theory. The AEM fails to reproduce the low-T behavior of both T_1 and T_2.

VII. DISCUSSION AND CONCLUSIONS

It is clear from the experimental results presented and the impact model theory developed to explain them, that nuclear magnetic relaxation in magnetically "tagged" superionic conductors is sensitive to the topological aspects of the random walk and to the details of the interaction during the encounter period. Despite the seemingly complex dependence that the relaxation has on the various parameters that enter into the model theory, an overall simple physical picture can be given by the observed behavior of T_2^{-1} and T_1^{-1} as a function of temperature.

That $T_1 = T_2$, with both proportional to W, at low temperatures follows directly from the fact that complete relaxation of the transverse and longitudinal ^{19}F magnetizations occurs in a *single* encounter with a Mn^{2+} spin in this region. With increasing temperature (or W), we pass from the region of single encounter to the region of multiple encounter relaxation. Whereas in the former, the relaxation rates increase as W (proportional to the rate of encounter), they decrease as W^{-1} (motional narrowing) in the latter region; a peak occurs where the transition takes place, with the approximate peak position given by the relation $W_{\text{peak}}^2 \simeq \frac{1}{3}A^2S(S+1)$. The interaction strength A in T_2^{-1} has contributions from both A_s and A_p, and is predominantly determined by A_s, which is the larger of the two. However, for the initial peak in T_1^{-1}, the effective interaction $A = A_p \ll A_s$, so this peak occurs at lower temperature than does that in T_2^{-1}. The high-temperature peak in T_1^{-1}, and $T_1^{-1} \propto \omega_e^{-1}$ appears when W becomes comparable with ω_e. At this point the power spectrum of the local field fluctuations centered at $\omega = \omega_e$, arising from the terms involving $A(I^+S^- + I^-S^+)$, develops appreciable intensity at *nuclear* Larmor frequencies and induces relaxation. If W eventually becomes much greater than ω_e, then a further decline in T_1^{-1} is predicted at the highest temperatures, as is observed experimentally at low fields (relatively small ω_e).

It is to be noted that the low-temperature region, where $T_2^{-1} = T_1^{-1} \simeq cW$ and is independent of the coupling constants, has not been observed before in NMR in condensed matter systems. As we have emphasized, this is closely connected with the nonperturbative character to the hard collision that each ^{19}F nucleus experiences in its encounter with a Mn^{2+} spin. For materials (e.g., CaF_2) where W increases more slowly with temperature, this regime might be quite extended and provide a direct means of studying the assumed diffusion mechanism, since only topological considerations enter into the relaxation rates. We were led to an understanding of this region by the obvious analog with the broadening of optical spectra in gases, where Kubo has shown[13] the impact approximation leads to a dependence of linewidths on the collision cross section and mean velocity, but *not* on the detailed coupling of the atom-atom interaction.

While the impact model theory provides a semiquantitative explanation of the experimental observations, there are significant discrepancies between the two, both in the shape of the high-temperature side of the initial peak in T_1^{-1}, and in the behavior of T_2^{-1} above its peak value. It is worth restating that the model theory has several essential simplifying assumptions: we have assumed the ion hops in an empty lattice and we have neglected all cooperative or collective effects that ensue if the density of mobile ions approaches the lattice site density. We have characterized the F^- ion motion in terms of the average hopping rate as determined from the low-frequency conductivity $\sigma(\omega=0,T)$. In addition, in treating T_1^{-1} in the impact approximation, we have assumed an angularly *averaged* value for the anisotropic interaction and thereby neglected the variation it often has as the ion hops from site to site within the active cell.

In the region below 550 K it is unlikely that collective effects are responsible for any discrepancies occurring in T_1^{-1}, since T_2^{-1} appears to be well described by the model theory up to this temperature. Furthermore, the properties of T_1^{-1}, $T_{1\rho}^{-1}$, and T_2^{-1} are all adequately given[8] in nominally pure PbF_2 below 550 K, if one describes the nuclear dipole-induced relaxation in terms of the same conductivity-determined hopping rate W and neglects collective mobile ion-ion effects. These various facts suggest that the discrepant behavior in T_1^{-1} between 400 and 650 K is associated with the sensitivity of T_1^{-1} to the relative magnitudes of τ_{sl}^{-1} and W, particularly in this region where they are approximately equal. More than a single encounter is required to relax the nuclear spin, so the amount of the average relaxation per encounter is important (in contrast with lower temperatures), and we must look more closely at the motion *within* an active cell. When τ_{sl}^{-1} is no longer larger than the hopping rate W, the electronic spin memory persists during jumps between active sites within the

same cell. Such a jump involves a change in the Mn-F axis relative to the external field, in general, and therefore in the anisotropic hyperfine components $A_{\alpha z}$. Under the assumed conditions these are modulated approximately at the rate W, whereas in the calculation above we have taken an *averaged* anisotropic interaction modulated at a rate $\nu + W/2$ ($\simeq W/2$ in this region) associated with motion on to and off of an active *cell*. Although we have been unable to incorporate this effect into the theory in detail, this discussion suggests that it would lead to a reduction in T_1^{-1} on the order of a factor of 2, which would bring the theory into closer agreement with experiment. Note that at higher temperatures, where the isotropic hyperfine interaction becomes important, the hopping rate $W/2$ from an active cell *is* the appropriate modulation rate, and agreement of theory and experiment in this region is not destroyed by the above considerations. For the same reason T_2^{-1} is not affected.

The high-temperature behavior of T_2^{-1} is more difficult to explain, especially in view of the general good agreement that is found for T_1^{-1} at three different frequencies in this same region. Here one must invoke the arguments appropriate to the power spectrum $P(\omega)$ of the local field fluctuations. The T_2^{-1} results, which are sensitive to $P(\omega)$ at $\omega = 0$, indicate that $P(\omega)$ for $\omega << 8$ MHz (which is the lowest frequency at which T_1^{-1} was measured) is anomalously large. This may be indicative of some very low-frequency collective mode peculiar to the truly superionic region, as was first suggested by Boyce *et al.*[8] in their NMR experiments in "pure" PbF_2. We use the phrase "pure" guardedly because there is abundant evidence from our original linewidth studies that much of what was observed in the original experiments on PbF_2 would be explained by inadvertent magnetic "tagging," at the level of 1 ppm.

ACKNOWLEDGMENTS

This research was supported in part by the Department of Energy, Contract No. DOE E34 PA-244 and by NSF Grant No. DMR 80-08004. The authors gratefully acknowledge discussions with Dr. Alan King, Professor Ryogo Kubo, Dr. Ingo Peschel, and Dr. Peter Richards. Mr. Neil Nighman has prepared all of the PbF_2 samples and has helped with confinement problems.

APPENDIX: THE COMPONENTS OF THE ^{19}F hfs TENSOR $\tilde{A}$

In the PbF_2 structure the Mn-F bonds lie along the four equivalent [111] directions. In this case $\tilde{A}$ may be expressed as the sum of scalar (A_s) and dipolar-like (A_p) terms. Choosing a coordinate system (X,Y,Z) with the Z axis collinear with a particular [111] direction, one finds $\tilde{A} = A_s + A_p(3\cos^2\theta - 1)$ with θ measured with respect to the Z axis. $\tilde{A}$ is diagonal in this reference system with $A_{\parallel} = A_s + 2A_p$ and $A_{\perp} = A_s - A_p$.

The laboratory reference frame (x,y,z), with $\vec{H}_0 = H_0\hat{z}$, will in general be oriented at random with respect to the bond coordinate system (X,Y,Z) in a polycrystalline material. $\tilde{A}$ in the laboratory frame is related to $\tilde{A}$ in the (X,Y,Z) frame by the transformation $\tilde{A}(x,y,z) = R^{-1}\tilde{A}(X,Y,Z)R$, where the matrix R is a function of the direction cosines that relate (x,y,z) and (X,Y,Z).

The components of the spherical tensor $A_{\alpha\beta}$ ($\alpha,\beta = \pm 1, 0$) are linear combinations of the A_{ij} ($i,j = x,y,z$) and are defined by

$$\begin{aligned} A_{00} &= A_{zz} \ , \\ A_{11} &= A^*_{-1-1} = \tfrac{1}{4}(A_{xx} - A_{yy} - i2A_{xy}) \ , \\ A_{1-1} &= A^*_{-11} = \tfrac{1}{4}(A_{xx} + A_{yy}) \ , \\ A_{10} &= A^*_{-10} = A_{01} = A^*_{0-1} = \tfrac{1}{2}(A_{zx} - iA_{yz}) \ , \end{aligned} \tag{A1}$$

where $(*)$ indicates the complex conjugate. In the perturbation theory, the angular averaged quantities

$$\langle |A_{\alpha\beta}|^2 \rangle = \frac{1}{4\pi}\int_0^{2\pi} d\phi \int_{-1}^{1} d(\cos\theta) A_{\alpha\beta}A^*_{\alpha\beta} \tag{A2}$$

are required. Performing these averages yields

$$\begin{aligned} \langle |A_{00}|^2 \rangle &= A_s^2 + \tfrac{4}{5}A_p^2 \ , \\ \langle |A_{1-1}|^2 \rangle &= \tfrac{1}{4}(A_s^2 + \tfrac{1}{5}A_p^2) \ , \\ \langle |A_{10}|^2 \rangle &= \langle |A_{11}|^2 \rangle = \tfrac{3}{10}A_p^2 \ . \end{aligned} \tag{A3}$$

The G_α of Eq. (5.3) are given by

$$\begin{aligned} G_z(t) &= \tfrac{4}{3}S(S+1)e^{-t/\tau_{sl}}\{\langle |A_{01}|^2\rangle \cos(\omega_0 t) + 2\langle |A_{11}|^2\rangle \cos[(\omega_e - \omega_0)t] + 2\langle |A_{1-1}|^2\rangle \cos[(\omega_e + \omega_0)t]\} \ , \\ G_{\pm}(t) &= \tfrac{1}{3}S(S+1)e^{-t/\tau_{sl}}(\langle |A_{00}|^2\rangle + 2\langle |A_{01}|^2\rangle e^{\pm i\omega_0 t} \\ &\quad + 4\langle |A_{11}|^2\rangle e^{\pm i(\omega_e - \omega_0)t} + 4\langle |A_{1-1}|^2\rangle e^{\pm i(\omega_e + \omega_0)t} + 2\langle |A_{10}|^2\rangle e^{\pm i\omega_e t}) \ , \end{aligned} \tag{A4}$$

where ± 1, 0 refer to the transverse and longitudinal components with respect to the quantization axis determined by the external field.

*Based in part on the Ph.D. thesis of S.P.V. (University of California, Santa Barbara, 1980) (unpublished).
†Based in part on the Ph.D. thesis of P.T. (University of California, Santa Barbara, 1981) (unpublished).
‡Present address: Effects Technology, Inc., Goleta, Calif.

[1]M. S. Whittingham and B. G. Silbernagel, in *Solid Electrolytes: General Principles, Characterization, Materials, Applications,* edited by P. Haggenmuller and W. van Gool (Academic, New York, 1977).
[2]P. M. Richards, in *Topics in Current Physics, Physics of Superionic Conductors,* edited by M. B. Salamon (Springer, Berlin, 1979).
[3]R. D. Hogg, S. P. Vernon, and V. Jaccarino, Phys. Rev. Lett. 39, 481 (1977).
[4]R. D. Hogg, S. P. Vernon, and V. Jaccarino, in *Fast Ion Transport in Solids, Electrodes and Electrolytes,* edited by P. Vashishta, J. N. Mundy, and K. G. Shenoy (North-Holland, New York, 1979).
[5]S. P. Vernon, Ph.D. thesis (University of California, Santa Barbara, 1980) (unpublished).
[6]R. T. Harley, W. Hayes, A. J. Rushworth, and J. F. Ryan, J. Phys. C 8, L530 (1975).
[7]R. Benz, Z. Phys. Chem. Neve. Folge 95, 25 (1975).
[8]J. B. Boyce, J. C. Mikkelson, Jr., and M. O'Keefe, Solid State Commun. 21, 955 (1977).
[9]H. M. Dickens, W. Hayes, C. Smith, and M. T. Hutchins, in *Fast Ion Transport in Solids,* edited by P. Vashishta, J. N. Mundy, and G. K. Shenoy (North-Holland, New York, 1979).
[10]C. Evora and V. Jaccarino, Phys. Rev. Lett. 39, 1954 (1977).
[11]P. M. Richards, Phys. Rev. B 18, 6358 (1978).
[12]R. Kubo and K. Tomita, J. Phys. Soc. Jpn. 9, 888 (1954).
[13]R. Kubo, in *Fluctuation, Relaxation and Resonance in Magnetic Systems,* edited by D. Ter Harr (Plenum, New York, 1962).
[14]G. R. Khutsishvily, Sov. Phys. JETP 3, 382 (1957) [Zh. Eksp. Teor. Fiz. 31, 424 (1956)].
[15]P. G. DeGennes, J. Phys. Chem. Solids 7, 345 (1958).
[16]W. E. Blumberg, Phys. Rev. 119, 79 (1960).
[17]R. D. Hogg, S. P. Vernon, and V. Jaccarino, Solid State Commun. 23, 781 (1977).
[18]S. P. Vernon and V. Jaccarino (unpublished).
[19]Matheson Coleman and Bell, Mfg. Chemists.
[20]J. M. Blocker, in *High Temperature Technology,* edited by I. E. Campbell (Wiley, New York, 1956).
[21]R. S. Hayano, Y. J. Uemura, J. Imayato, N. Nishida, T. Yamazaki, and R. Kubo, Phys. Rev. B 20, 850 (1979).
[22]G. A. Samara, J. Phys. Chem. Solids 40, 509 (1979).
[23]S. P. Vernon and A. R. King, Phys. Rev. B 24, 3772 (1981), paper II.
[24]E. Dormann, D. Hone, and V. Jaccarino, Phys. Rev. B 14, 2715 (1976).